JACS
JOURNAL OF THE AMERICAN CHEMICAL SOCIETY
Article
pubs.acs.org/JACS

Heme Reactivity is Uncoupled from Quaternary Structure in Gel-Encapsulated Hemoglobin: A Resonance Raman Spectroscopic Study

Eric M. Jones, Gurusamy Balakrishnan, and Thomas G. Spiro*

Department of Chemistry, University of Washington, Box 351700, Seattle, Washington 98195-1700, United States

Supporting Information

ABSTRACT: Encapsulation of hemoglobin (Hb) in silica gel preserves structure and function but greatly slows protein motion, thereby providing access to intermediates along the allosteric pathway that are inaccessible in solution. Resonance Raman (RR) spectroscopy with visible and ultraviolet laser excitation provides probes of heme reactivity and of key tertiary and quaternary contacts. These probes were monitored in gels after deoxygenation of oxyHb and after CO binding to deoxyHb, which initiate conformational change in the R−T and T−R directions, respectively. The spectra establish that quaternary structure change in the gel takes a week or more but that the evolution of heme reactivity, as monitored by the Fe−histidine stretching vibration, ν_{FeHis}, is completed within two days, and is therefore uncoupled from the quaternary structure. Within each quaternary structure, the evolving ν_{FeHis} frequencies span the full range of values between those previously associated with the high- and low-affinity end states, R and T. This result supports the tertiary two-state (TTS) model, in which the Hb subunits can adopt high- and low-affinity tertiary structures, *r* and *t*, within each quaternary state. The spectra also reveal different tertiary pathways, involving the breaking and reformation of E and F interhelical contacts in the R−T direction but not the T−R direction. In the latter, tertiary motions are restricted by the T quaternary contacts.

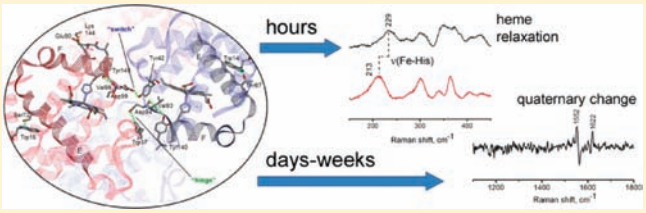

INTRODUCTION

The mechanism of protein allostery remains a challenging problem in structural biology. Alternative end structures are known in atomic detail for many proteins, but how allosteric transitions occur and how they are linked to function is not fully understood. Hemoglobin (Hb), the paradigmatic allosteric protein, continues to offer the best platform for developing mechanistic insight, because of its favorable physicochemical characteristics and because of its extensive database of structure and function.

Hb has long provided a template for other allosteric proteins via the celebrated two-state model of Monod, Wyman, and Changeux (MWC),[1] combined with Perutz' historic crystal structures.[2,3] This model[4−6] explained cooperative ligand binding as resulting from rearrangement of the four Hb subunits (two α and two β chains) from a low-affinity ("tense") structure, T, to a high-affinity ("relaxed") structure, R. The R and T forms are stable when ligand is bound or absent, respectively, with the transition occurring at an intermediate ligand occupancy. Allosteric effectors lower ligand affinity by stabilizing the T structure.

Crystallography reveals that the T-R transition principally consists of an ∼15° rotation of one $\alpha\beta$ dimer against the other.[4] Several salt bridges and interdimer hydrogen bonds that stabilize the T state are broken in forming the R state. Numerous R-state structures have been observed in crystals,[7] but these structures are similar in energy and have been shown by NMR to interconvert in solution.[8−11]

While the MWC model has successfully accounted for a wide range of equilibrium and kinetic ligand binding data, violations of the model have accumulated over the years and have motivated a series of elaborations and modifications.[12] The latest of these is the tertiary two-state (TTS) model, formulated by Eaton and co-workers,[13] some features of which were anticipated earlier by Lee and Karplus.[14] In this model, the Hb subunits can adopt alternative high- and low-affinity tertiary structures, *r* and *t*, whose populations are biased by the quaternary structure. The notion that Hb affinity may be linked to tertiary structure has also been demonstrated by Yonetani's observations[15] that allosteric effectors modulate ligand affinity within both quaternary structures. The TTS model contradicts the central tenet of the MWC allosteric models: that ligand affinity is strictly linked to quaternary structure.

In our laboratory and others, the allosteric pathway from R to T has been studied via pump−probe spectroscopy of the CO adduct, COHb, revealing several kinetic intermediates.[16−26] These studies have shown that quaternary structure change is not concerted but occurs in two distinct steps, with time constants of ∼2 and ∼20 μs (only the latter had previously been recognized, from kinetic studies of ligand rebinding[19,21]). UV resonance Raman (UVRR)[16] and CD[23] spectroscopy identified the two steps with formation of separate T quaternary contacts between opposite C helices and FG corners of the two subunits, α and β, at the $\alpha_1\beta_2$ interface.

Received: October 27, 2011
Published: January 22, 2012

 © 2012 American Chemical Society dx.doi.org/10.1021/ja210126j | J. Am. Chem. Soc. 2012, 134, 3461−3471

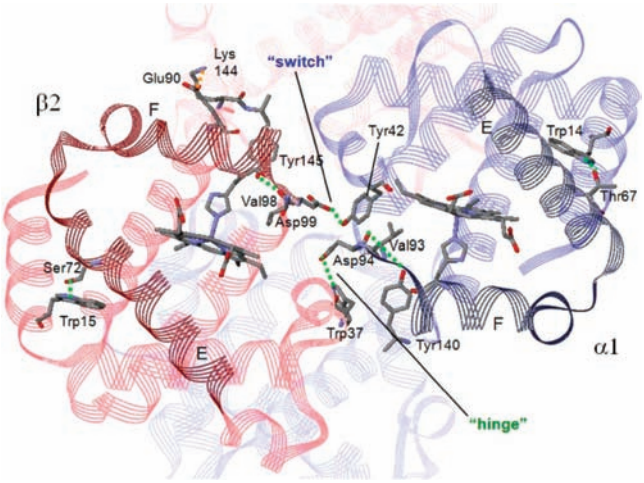

Figure 1. View of the interdimer $\alpha_1\beta_2$ interface of T-state Hb (PDB ID 1A3N), with α chains in blue and β chains in red. The backbone trace in the "allosteric core" (E and F helices and FG-corner) is shown in a darker shade. UVRR-sensitive H-bonded probes at the tertiary (A–E and F–H helices) and quaternary (hinge and switch) contacts are labeled (hydrogen bonds are shown as dashed green lines).

These have been called the "hinge" and "switch" contacts (Figure 1), the hinge involving a reorientation, and the switch involving an altered interdigitation of the contacting side chains.[4] Wide angle X-ray scattering (WAXS) measurements[27] indicate that the main structural rearrangement occurs during the first quaternary phase, at ~2 μs (see ref 28 for a synopsis of these experimental developments). The finding of two quaternary steps strikingly supports a new computational result from Karplus and co-workers,[29] who applied the conjugate peak refinement (CPR) method[30] to find the minimum-energy pathway of the T-R transformation. Their simulation indicates that the 15° interdimer rotation actually proceeds in two steps, via quite different rotations, one based on the α chains and the other based on the $\alpha\beta$ dimers. The latter is the first rotation in the R-T direction and involves most of the quaternary change, consistent with the WAXS result. The CPR trajectory[29] also reveals a series of tertiary changes, before and after the quaternary changes, consistent with the TTS model. These findings make clear that the allosteric transition in Hb is more complex than initially envisioned.

The TTS model was largely inspired by experiments on Hb encapsulated in silica sol–gels.[31] The encapsulated Hb retains functionality and is accessible to the ligand in the bathing solution, but the gel greatly slows protein motion, thereby enabling observation of intermediates that may be inaccessible in solution. In sol–gels, the allosteric transition can be studied not only in the R-T direction (by deoxygenating encapsulated oxyHb) but also in the T-R direction (by adding ligand to encapsulated deoxyHb). The latter transition cannot readily be studied in solution, where ligand binding is slower than protein rearrangement. The gels are optically clear, allowing the protein to be monitored by absorption or Raman spectroscopy. The TTS assumption that low- and high-affinity tertiary structures coexist within each quaternary structure was prompted by CO recombination measurements showing both fast and slow recombination phases in T-state gels.[31] The rates were similar to those of R- and T-state tetramers in solution, but the gel retained the T structure on the time scale of the measurements. Thus the rates were reassigned to r and t tertiary structures within the T state.

These developments motivated the present gel experiments, in which we have monitored structure change during the R-T and T-R transitions, both at the heme group, using absorption and heme-resonant Raman spectroscopy, and at key aromatic residues in the protein, using UVRR spectroscopy. Absorption spectroscopy on Hb gels was pioneered by Shibayama and Saigo,[32] while Friedman and co-workers demonstrated the application of both visible and UVRR spectroscopy.[33−37] We find that heme reactivity, as monitored by the stretching frequency of the Fe–histidine bond, evolves much faster than do the markers of quaternary structure change in either the R-T or the T-R direction. This result implies that the ligand binding is controlled by tertiary structure, regardless of the quaternary structure, thus supporting the TTS model. However, the evolution of tertiary structure, as monitored by UVRR spectroscopy, differs in the R-T and T-R directions, indicating that tertiary change is channeled by the quaternary structure.

EXPERIMENTAL PROCEDURES

Materials. Hemoglobin A (Hb) was purified from human blood as described previously[38] and stored in the carbonmonoxy form (COHb) at −80 °C. Oxy- and deoxy-Hb were prepared from COHb by photolysis on ice under a stream of oxygen or argon, respectively, essentially as described in the literature.[39] Hb concentration was assessed by visible spectrophotometry of the Soret absorption band, using published values of heme absorptivity.[39] Tetramethyl orthosilicate (TMOS), sodium phosphate buffers, and inositol hexaphosphate (IHP) were purchased from Sigma, were of reagent grade, and were used without further purification. Sodium dithionite (Sigma) was of technical grade and was used within 6 months of purchase.

Encapsulation of Hb. Sol–gel encapsulation of Hb was performed essentially according to Khan et al.,[36] using phosphate buffer in place of bis-tris for consistency with earlier UVRR experiments from our laboratory. Briefly, 60 μL each of TMOS and 50 mM sodium phosphate (with or without 4.5 mM IHP, pH 6.5) were mixed in a sample tube and vortexed for ~2 min to initiate hydrolysis. When the mixture turned cloudy, 60 μL of hemoglobin solution in the same buffer was added, and the sample was vortexed for a further ~30 s. The tube was then rotated horizontally until the sol–gel hardened, typically in 5–10 min. These steps were performed under ambient conditions (for oxyHb gels) or under argon using degassed solutions (for deoxyHb gels). This procedure resulted in formation of a thin sol–gel film coating the inner surface of the sample tubes; the film thickness was estimated from visible absorption to be ~300–400 μm regardless of sample geometry. The sol–gel was then covered in the same buffer as above (saturated with O_2 or Ar for oxyHb or deoxyHb gels, respectively) and allowed to wet-age in the dark at 4 °C for 48 h under 1 atm O_2 (oxyHb) or Ar (deoxyHb) before use. The bathing buffer was changed once during this time to remove methanol and nonencapsulated protein. Visible spectrophotometry confirmed that formation of metHb was negligible (≤5%) under these conditions provided that the storage time did not exceed 48 h (data not shown). The final concentration of Hb in the sol–gels was 100 μM in heme for visible absorption experiments; for Raman experiments, the final concentration of Hb in sol–gels was 430 μM (deoxyHb) or 860 μM (oxyHb). The estimated chloride concentration was <2 mM in all samples.

Conversion of encapsulated oxyHb (R state) to deoxyHb was initiated by adding sodium dithionite to the bathing buffer of an oxyHb gel, using an Ar-purged syringe, to a final concentration of ~2 mM. Conversion of encapsulated deoxyHb (T state) to COHb was initiated by completely removing the bathing buffer of a deoxyHb gel and replacing it with CO-saturated buffer. Since the sample temperature cannot be precisely controlled in our experimental apparatus, all experiments were performed at 22 ± 0.5 °C.

Absorption Spectrophotometry. Samples for visible absorption spectroscopy were prepared in 1 cm glass vials mounted in the 8-chamber multicell holder of an Agilent 8453 diode-array UV−visible spectrophotometer. A vial containing only buffer served as blank. The change in absorption of the Soret difference band[32] was monitored as a function of time after addition of sodium dithionite to oxyHb gels (R to T conversion) or addition of CO-saturated buffer to deoxyHb gels (T to R conversion). Spectra were automatically collected every 2 min for the first 5 h of conversion, every 10 min for the next 20 h, and every 30 min thereafter. Each sample condition was monitored in triplicate and the results averaged.

Visible Resonance Raman Spectroscopy. Raman excitation light (426 nm, 1 kHz, 25 ns, 5.0 ± 0.2 μJ/pulse) was provided by the second harmonic of a Ti:sapphire laser (Photonics Industries International) pumped by the intracavity frequency-doubled output (527 nm) of a Q-switched Nd:YLF laser (GM30, Photonics Industries). Excitation light was focused on a spinning 5 mm glass NMR tube containing the sol−gel sample; scattered light was collected at 135° by a camera lens and focused onto the 0.2 mm entrance slit of a two-stage spectrometer (Spex Triplemate 1877) equipped with a 2400 groove/mm holographic grating (at the spectrograph stage) and a liquid N_2-cooled charge-coupled device (CCD) detector (Roper Scientific, Inc.). Spectra were accumulated for 2 min and calibrated using standard Raman spectra of dimethylformamide. The COHb photoproduct yield was measured using the ν_4 band intensity of deoxy heme at 1355 cm^{-1} as reported previously in solution studies.[16,20,40] The NMR tubes containing the gel samples were spun and translated up and down during the acquisition of spectra to avoid multiple excitation of the same gel spot (see below).

Ultraviolet Resonance Raman Spectroscopy. The equipment used for ultraviolet resonance Raman spectroscopy has been described elsewhere.[41] Excitation (229 nm, 1 kHz, 20 ns, 1.4 μJ/pulse) was from the fourth harmonic of a Photonics Industries Ti:sapphire laser pumped by the frequency-doubled output (527 nm) of a Q-switched Nd:YLF laser (DDC Technologies, Inc.). The excitation laser was focused to a line, using a cylindrical quartz lens, on a spinning 7 mm quartz NMR tube containing the sol−gel. Scattered light was collected at 135° by a quartz lens and focused on the 0.2 mm entrance slit of a 1.26 m spectrometer equipped with a 3600 groove/mm holographic grating and a liquid N_2-cooled, UV-optimized CCD detector (Princeton Instruments). Spectra were calibrated using the standard Raman spectrum of acetone.

Because sol−gel samples cannot be stirred, encapsulated Hb was highly sensitive to decomposition in the UV laser, as evidenced by rapid loss of spectral intensity (particularly of tryptophan (Trp) bands) during acquisition (data not shown). To minimize sample degradation, the sample holder was mounted on a motorized stage (ThorLabs APT, drive motor model Z812), which cyclically translated the sample tube (1 mm/s, 8-mm vertical travel length), while it was simultaneously spun at >500 rpm. The laser beam was blocked when acquisition was not being performed. Using this arrangement, a given 8 mm zone could be irradiated for up to 2 min with 1.4 ± 0.1 mW excitation before loss of Trp peak intensity became evident. Spectra were accumulated at each of six zones, each zone representing a different time interval, and spectra were averaged for 2−4 replicate samples. Samples were kept in the dark at 22 °C between measurements. The normal UVRR intensity standards, perchlorate and sulfate ions, could not be used because partitioning of the salt into the bathing solution lowered the intensity in the gel and because the gel itself has a high background in the spectral region (800−1000 cm^{-1}) of the anion signals. Instead, the broad water band was used as the standard, and UVRR difference spectra were generated by subtraction to give a flat baseline from 1500 to 1800 cm^{-1}. The reliability of this procedure is validated by the good agreement between solution and gel difference spectra of deoxyHb minus COHb (Supporting Information Figure S1)

Data Analysis. Raman spectra were processed using Grams/AI v7.00 (Thermo Galactic Industries). In heme-RR spectra, peak positions were determined by least-squares fitting of a Gaussian band to the peak of interest; the uncertainty in peak position is ±1 cm^{-1}. Multiple samples were averaged for each time point, and the averaged difference spectrum was interactively baseline-corrected. UVRR difference spectra were further smoothed using a nine-point Savitsky-Golay binomial function. The uncertainty in UVRR peak positions is estimated at ±2 cm^{-1}.

Curve-fitting of absorption and vis-RR time courses was performed in Microcal Origin v6.0 Software. Time traces were successively fit to a sum of one, two, or three exponentials using a common set of initial conditions and a fixed final value of the dependent variable. Acceptance or rejection of more complex functions was based on the Fisher F-test, using $P \leq 0.05$ for the appropriate number of degrees of freedom, taken from standard tables.[42] Error surfaces for time constants (minimum χ^2 possible for various fit values) were calculated by performing the multiexponential fits described above with each successive time constant separately fixed, essentially as described by Beechem and Haas.[43]

RESULTS

Spectroscopic changes in gel-encapsulated Hb were monitored in two sets of experiments. In the first set, the R-T sequence oxyHb was rapidly deoxygenated with dithionite,[32] producing deoxyHb in the R quaternary state, which then gradually converted to the equilibrium T quaternary state. In the second set, the T-R sequence deoxyHb was exposed to CO-containing buffer, producing COHb in the T quaternary state, which gradually converted to the equilibrium R quaternary state.

Spectroscopic markers were chosen to reveal different aspects of Hb dynamics. Heme absorption spectra were monitored to ensure consistency with previous reports of Hb kinetics in sol−gel.[32] The heme Soret absorption band is sensitive to the heme environment, averaging the effects of the surrounding structure.

Raman spectra provide specific structural information. RR excitation at visible wavelengths near the Soret absorption band produce enhanced vibrational bands of the heme chromophore. These include the ligation-dependent porphyrin breathing mode, ν_4,[44,45] which provides a convenient quantitative monitor of ligation status. Soret-resonant excitation also enhances the $\nu_{Fe\text{-}His}$ mode that is responsive to the stretching of the bond between the heme Fe and the proximal histidine ligand[46] and is a monitor of heme reactivity (see below). However, this mode is observable only for 5-coordinate deoxy-heme. It is not enhanced for 6-coordinate heme.[47] The $\nu_{Fe\text{-}His}$ frequency reflects the strength of the Fe−His bond. This frequency is substantially lower in deoxyHb than in deoxy-myoglobin or in separated Hb subunit dimers,[17,48,49] a difference thought to reflect molecular tension in the T state. In agreement with Friedman et al.,[33−36] we found no difference between $\nu_{Fe\text{-}His}$ bands recorded in solution or in gels, for either deoxyHb or for the COHb photoproduct (Figure S2 of the Supporting Information), establishing that gel encapsulation does not affect this important structural marker.

RR excitation in the ultraviolet enhances vibrational bands of UV chromophores within the protein.[50−52] In particular, RR spectra with 229 nm excitation mainly contain bands of tyrosine (Tyr) and tryptophan (Trp) residues. The intensities and in some cases the frequencies of these bands are sensitive to the residue environments, and particularly to hydrogen bond interactions.[51] H-bonds from Tyr and Trp form key tertiary and quaternary contacts in Hb, for which characteristic UVRR signals have been identified.[16,53−56]

1. R-T Sequence: Deoxygenation of Encapsulated oxyHb. *a. Soret Absorption Band.* Immediately after deoxygenation, the deoxy-heme Soret band is centered at 431

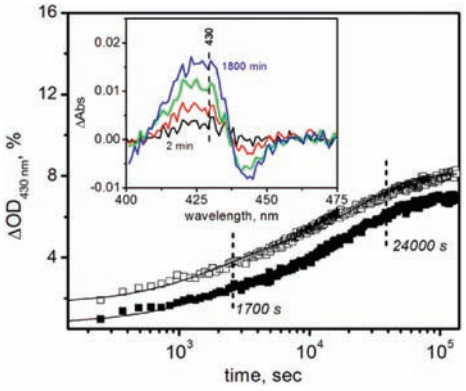

Figure 2. Time course of visible absorption change (430 nm) following removal of O_2 from oxyHb gels in the absence (filled symbols) or presence (open symbols) of IHP. Solid lines are fits to a double exponential with time constants indicated by dotted lines. Inset, Soret difference spectra obtained by subtracting the initial ($t \approx 0$) deoxyHb spectrum from the deoxyHb spectra at 2 min (black), 30 min (red), 3 h (green), and 30 h (blue) after removal of O_2.

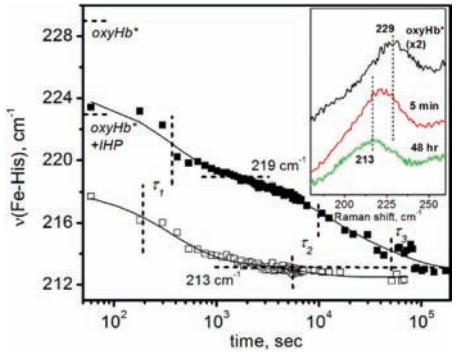

Figure 3. Time course of shift in $\nu_{Fe\text{-}His}$ after removal of O_2 from oxyHb gels in the absence (filled symbols) or presence (open symbols) of IHP. Solid lines are fits to a sum of exponentials with time constants (τ_1–τ_3) indicated with vertical dashed lines (see Table 1). Horizontal dashed lines at the left indicate the position of $\nu_{Fe\text{-}His}$ in the initial oxyHb photoproduct; that at the bottom indicates the equilibrium (T-state) $\nu_{Fe\text{-}His}$ for deoxyHb. Inset, the $\nu_{Fe\text{-}His}$ bands of oxyHb photoproduct (black) and deoxyHb at 5 min (red) and at 48 h (green) after removal of O_2.

nm and then shifts to slightly shorter wavelengths and intensifies. Figure 2 shows successive difference spectra, and the time dependence of the positive difference band, monitored at 430 nm. Intensification is complete within 30 h, and the time-course can be fit by two exponentials, with time constants of 1.70 ± 0.06 and 24.1 ± 0.4 × 10^3 s (0.5 and 6.7 h, respectively), with amplitudes of 22 and 78% (of a total absorbance change of 8%), after a rapid change (due mainly to deligation) within the ~2 min dead time of the experiment. Similar results were first reported by Shibayama and Saigo,[32] albeit with different time constants of 0.2, 1.5, and 19 h. The slightly altered kinetics likely reflects differences in the encapsulation protocol and the higher pH (7.0 vs 6.5) used in their study.[32]

Co-encapsulation of the effector molecule inositol hexaphosphate (IHP, 4.5 mM) to the sample did not alter the kinetics but did increase the extent of the absorption change slightly. This increase was evident immediately after deoxygenation and persisted over the entire time course (Figure 2).

b. $\nu_{Fe\text{-}His}$ Raman Band. The deoxy-heme $\nu_{Fe\text{-}His}$ RR band was recorded with 426 nm excitation, and its frequency, obtained by band fitting, was monitored (Figure 3). Immediately after deoxygenation, the frequency is 224 cm^{-1}, similar to that observed for myoglobin or for Hb $\alpha\beta$ dimers.[17] Within 48 h, the frequency decreases to 213 cm^{-1}, the value seen for deoxyHb at equilibrium. Fitting the time course requires three exponentials, with time constants of 0.1, 2.8, and 15 h, and corresponding frequency shifts of 5, 3, and 3 cm^{-1} (Table 1). Similar results have been reported by Friedman and co-workers.[57] The RR spectrum of oxyHb prior to deoxygenation also contains a deoxy-heme $\nu_{Fe\text{-}His}$ band, due to partial photolysis in the laser beam, with a significantly elevated frequency, 229 cm^{-1}. This 5 cm^{-1} elevation is attributed to Fe–His bond compression produced when photolysis drives the Fe toward the proximal F-helix, which is constrained by the protein structure.[20]

In contrast to the absorption spectral changes, a large effect of IHP is seen on the $\nu_{Fe\text{-}His}$ frequency. It is lowered by 5–6 cm^{-1} in the oxyHb photoproduct and in the deoxy-heme immediately after deoxygenation. It then decreases rapidly (0.05 and 1.5 h time constants, with 5 and 1 cm^{-1} shifts) to 212 cm^{-1}, essentially the same deoxyHb equilibrium value seen without IHP.

Table 1. Time Constants for Heme Relaxation from vis-RR Spectra[a]

	[b]τ_1, sec × 10^3	τ_2, sec × 10^3	τ_3, sec × 10^3
oxyHb − O_2			
$\nu_{Fe\text{-}His}$ −IHP	0.36 ± 0.04 (5)	10 ± 3 (3)	54 ± 14 (3)
$\nu_{Fe\text{-}His}$ +IHP	0.19 ± 0.03 (5)[c]	5.4 ± 0.6 (1)	
deoxyHb + CO (photoproduct)			
$\nu_{Fe\text{-}His}$ −IHP	0.29 ± 0.06 (4)	18.0 ± 3.6 (3)	79 ± 22 (3)
$\nu_{Fe\text{-}His}$ +IHP	0.54 ± 0.11 (3)	18.3 ± 1.2 (6)	
ν_4 −IHP	0.14 ± 0.03 (0.18)[d]	5.0 ± 0.4 (0.11)	
ν_4 +IHP	0.18 ± 0.03 (0.12)	8.4 ± 0.6 (0.12)	

[a]Values given are best fit ± fitting error, with the respective amplitude in parentheses. [b]Amplitudes of $\nu_{Fe\text{-}His}$ frequency shifts (in cm^{-1}) are given parenthesis. [c]Amplitude includes an unresolved rapid phase. [d]Amplitudes of ν_4 relaxations represent fraction of deoxyheme (see text).

Error surfaces calculated for the kinetic fitting are shown in the Supporting Information (Figure S3). They indicate that the second and third time constants for the $\nu_{Fe\text{-}His}$ evolution overlap (within experimental uncertainty) with the two time constants determined from the absorbance experiment. Thus, the absorbance and Raman experiments are monitoring the same physical processes, but the time constants for shifts in $\nu_{Fe\text{-}His}$ are somewhat poorly defined.

c. UVRR Markers of Tertiary and Quaternary Structure. UVRR difference spectra following deoxygenation of oxyHb (Figure 4) show the evolution of tertiary and quaternary structure markers, which have been well documented in pump–probe solution studies of COHb photodissociation.[16,20,25] UV laser damage (see Experimental Procedures) prevented spectral accumulation at enough time points for a quantitative kinetic analysis, but the sequence of UVRR changes is clear from the sampled time points.

Within three minutes, a negative difference band appears at 1562 cm^{-1}, representing the W3 mode of the interior Trp residues, α14 and β15.[54] Its intensity loss is due to the loss of tertiary H-bonds from these A helix residues to Thrα67 and

dx.doi.org/10.1021/ja210126j | J. Am. Chem. Soc. 2012, 134, 3461–3471

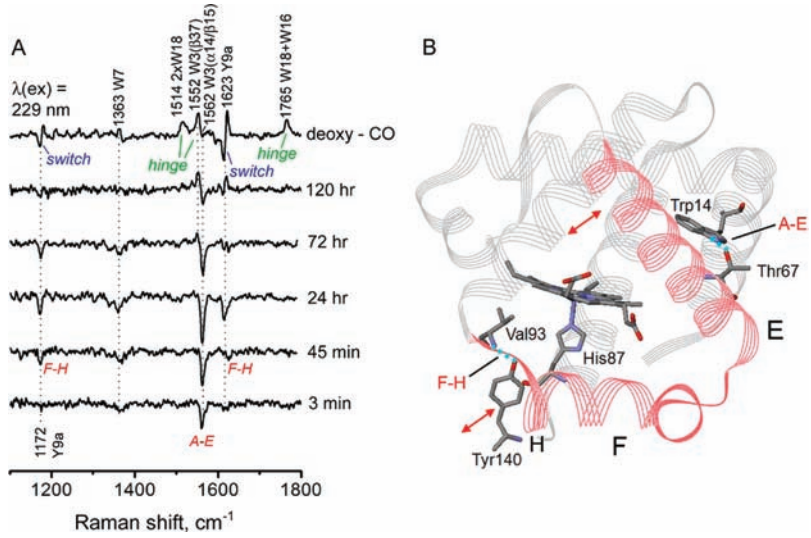

Figure 4. (A) UVRR difference spectra (deoxyHb minus oxyHb) collected at the indicated times during the R to T conversion in sol−gels. A static deoxy-minus-CO difference spectrum of Hb in sol−gel is provided at top for reference. Transient peaks assigned to breakage of the tertiary A−E and F−H helix H-bonds (shown in panel B) are labeled in red; the UVRR peaks assigned to the hinge and switch (interdimer) H-bonds are labeled in green and blue, respectively. (B) Location of internal hydrogen bonds (dotted cyan lines) in the α chain. Breakage of these bonds allows rotation of the E/F helix clamshell (red) in response to ligand departure from the distal pocket, in the direction indicated by double red arrows. See text for details.

Serβ68,[58] on the E helices of the two chains (see Figure 4 for a structural diagram of the α chains). In 45 min additional negative bands appear at 1619 and 1172 cm^{-1}, assignable to tyrosine Y8a and Y9a modes.[51] Their intensity loss is due to loss of a second set of tertiary H-bonds, donated from the H-helix residues Tyrα140 and Tyrβ145 to the backbone carbonyls of the F-helix residues Valα93 and Valβ98[59] (Figure 4). Loss of these tertiary H-bonds has been proposed[60−62] to result from concerted rotations of the E and F helices, which surround the heme like a clamshell (Figure 4), in response to deligation of the heme.

Of great interest is the present observation that the negative Trp signal precedes the negative Tyr signal, indicating that the A−E H-bond breaks before the F−H H-bond. In solution, the two events were not resolved in pump−probe measurements, both occurring on the nanosecond time scale.[16] However, similarly sequential E and F helix motions have been suggested for Mb from picosecond time-resolved UVRR spectroscopy.[63]

The negative Trp and Tyr bands continue to grow until 24 h, after which they diminish. This loss of the initial negative signals is seen as well in the solution pump−probe time course and has been suggested to reflect re-establishment of the interhelical H-bonds, en route to the formation of T-state intersubunit contacts.[16]

The UVRR markers for the T-state contacts are a pair of derivative-shaped Tyr bands at 1620 and 1175 cm^{-1} (Y8a and Y9a) and positive Trp bands for the W3 mode at 1552 cm^{-1} (distinctly lower than the 1562 cm^{-1} W3 mode of the α14 and β15 residues and assignable to the Trpβ37 residue[54]) and the W18 overtone[64] (1514 cm^{-1}) and combination (with W16, at 1767 cm^{-1}) modes. These can all be seen in the deoxyHb-COHb static difference spectrum (Figure 4). A series of isotopic substitution and mutational studies[16,53−56,58] have shown these signals to arise from intersubunit H-bonds at the hinge and switch contacts in the T-state. The "hinge" H-bond is from Trpβ37 to Aspα94, while the "switch" H-bond is from Tyrα42 to Aspβ99 (Figure 1).

Both sets of signals appear in the sol−gel difference spectra after the tertiary signals have diminished, as they do in solution pump−probe studies. But even at 120 h (5 days), they have not reached the full amplitude seen in the static deoxyHb-COHb difference spectrum. At 72 h, one can see a weak "hinge" contact, before the appearance of the "switch" contact. This sequence agrees with the pump−probe solution studies, in which the time-constants for the "hinge" and "switch" contact formation differ by a factor of 10.[53] The limited time resolution in the gels prevents a quantitative assessment of this rate difference; formation of metHb after ∼5 days of storage prohibited monitoring of the R-T conversion out to longer time periods.

The data of Figures 3 and 4 establish that the $\nu_{\text{Fe-His}}$ band evolves on the same time scale as the tertiary UVRR signals and that this evolution is complete well before the T quaternary UVRR signals appear. Surprisingly, although IHP has a considerable effect on the relaxation of $\nu_{\text{Fe-His}}$ in vis-RR spectra (Figure 3), it has negligible effect on UVRR spectra and on the rates of appearance of UVRR difference signals. UVRR difference spectra of samples containing 4.5 mM IHP are essentially indistinguishable from those shown in Figure 4A (and are therefore not shown.)

2. T-R Sequence: CO Binding to Encapsulated deoxyHb. *a. Soret Absorption Band.* The absorbance change following CO ligation to deoxyHb (Figure 5) is smaller than that following deoxygenation of oxyHb, perhaps because the CO-bound 6-coordinate heme is more rigid than the 5-coordinate deoxy-heme and may be less responsive to environmental changes. However, the time course of the change is similar and can again be fit with two exponentials with similar time constants, 1.1 and 12.6 × 10^3 s (45 and 55% amplitudes). Again IHP has no effect on the kinetics but reduces the absorbance change slightly at all time points.

b. $\nu_{\text{Fe-His}}$ Raman Band. Soret-enhanced RR spectra of COHb contain a $\nu_{\text{Fe-His}}$ band (Supporting Information Figure S2), which arises from the deoxy-heme that is transiently generated

dx.doi.org/10.1021/ja210126j | J. Am. Chem. Soc. 2012, 134, 3461−3471

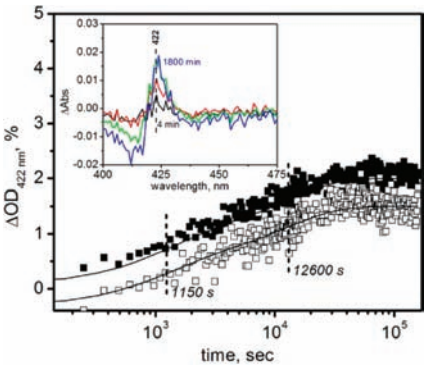

Figure 5. Time course of visible absorption change (422 nm) following addition of CO to deoxyHb gels in the absence (filled symbols) or presence (open symbols) of IHP. Solid lines are fits to a double exponential with time constants indicated by dotted lines. Inset, Soret difference spectra obtained by subtracting the initial ($t \approx 0$) COHb spectrum from the COHb spectra at 4 min (black), 40 min (red), 5 h (green), and 30 h (blue) after addition of CO.

by the probe laser. Its frequency, ~230 cm^{-1}, is elevated relative to Mb or relaxed forms of Hb (~224 cm^{-1}), an effect attributed to compression of the Fe−His bond, as discussed above. Since CO recombination is rapid, the band represents the steady state population of transient deoxy-heme maintained by the probe laser flux. The RR spectrum has contributions from photolyzed and unphotolyzed CO-heme. The latter gives rise to a $\nu_{Fe\text{-}CO}$ band at 503 cm^{-1} (Supporting Information Figure S2) and to a ν_{CO} band at 1949 cm^{-1}(not shown), the same frequencies seen in solution.[65]

A much lower photoproduct $\nu_{Fe\text{-}His}$ frequency, 219 cm^{-1}, is seen for gel-encapsulated deoxyHb immediately after CO binding (Figure 6). The band shifts back toward the R state

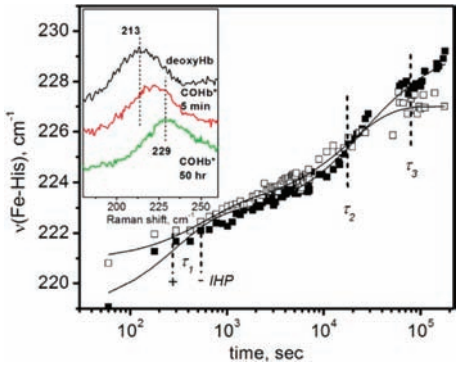

Figure 6. Time course of shift in $\nu_{Fe\text{-}His}$ after addition of CO to deoxyHb gels in the absence (filled symbols) or presence (open symbols) of IHP. Solid lines are fits to a sum of exponentials with time constants (τ_1−τ_3) indicated with vertical dashed lines (see Table 1). Inset, the $\nu_{Fe\text{-}His}$ bands of deoxyHb (black) or COHb photoproduct at 5 min (red) or at 50 h (green) after addition of CO.

value, 230 cm^{-1}, on the same time scale seen for $\nu_{Fe\text{-}His}$ relaxation in the R-T sequence following oxyHb deoxygenation (Figure 3). Indeed if a correction is made for the ~5 cm^{-1} photoproduct bond compression effect, the two $\nu_{Fe\text{-}His}$ time courses are almost mirror images. Three exponentials are again required to fit the evolution, and the time constants, 0.3, 18, and 79 × 10^3 s, are quite similar to those of the R-T sequence (within experimental error; Supporting Information Figure S3) as are the associated frequency shifts, 4, 3, and 3 cm^{-1}. Importantly, the time scale of the $\nu_{Fe\text{-}His}$ evolution is consistent with the observation by Ronda et al.[66] that the amplitude of the faster recombination phase (interpreted as belonging to *r* subunits) in the T-state COHb gel increased with time and reached completion in about a day.

However, the effect of IHP is dramatically different in the T-R and R-T sequences. Whereas IHP strongly lowers $\nu_{Fe\text{-}His}$ following oxyHb deoxygenation, it has little effect on CO-bound deoxyHb. The time courses with and without IHP are nearly superimposable (Figure 6), although the third phase is absent and the frequency levels off at a slightly lower value, 227 cm^{-1}.

Interestingly, the CO-heme $\nu_{Fe\text{-}CO}$ and ν_{CO} bands remain at the R-state COHb frequencies, 503 and 1949 cm^{-1}, throughout the T-R time course. These bands are known to be sensitive to alterations in the Fe−His bond, in various heme proteins.[67] Thus the evolution in protein structure does not affect the structure of the CO-heme but does affect the photoproduct deoxy-heme following CO dissociation.

c. CO-heme Photodissociation Yield. The steady state photoproduct population can be measured via the heme breathing mode, ν_4, which is the strongest band in the Soret-enhanced RR spectrum.[40,44,45] It shifts from 1355 to 1372 when deoxy-heme binds CO (Figure 7 inset), and the fraction of each

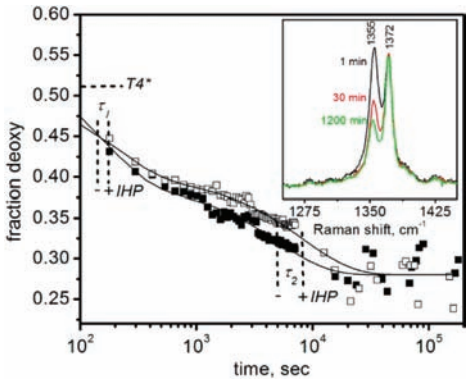

Figure 7. Time dependence of photoproduct yield (estimated from ν_4 band) following addition of CO to deoxyHb sol−gels in the absence (filled symbols) and presence (open symbols) of IHP. Solid lines are fits to a double exponential with time constants indicated by vertical dashed lines (see Table 1). The fraction of deoxyheme in the initial photoproduct (T4*) is indicated by the horizontal dashed line. Inset, ν_4 band of heme at 1 min (black), 30 min (red), and 1200 min (green) after CO addition, showing decrease in deoxy component with time.

species is straightforwardly determined from the known cross sections of deoxy- and COHb.[68] The deoxy fraction is ~50% immediately after addition of CO to the deoxyHb gel, but it decreases with time, reaching ~30%, the same fraction seen in COHb gels (R state). Importantly, this value is reached in about 3 h. The time course can be fit with two exponentials, having time constants of 0.1 × 10^3 and 5 × 10^3 s (Table 1). The steady-state deoxy-heme fraction represents the ratio of photodissociation and recombination rates. The photodissociation rate is constant, depending only on the probe laser flux. Thus the decline in the deoxy fraction results from an increase in recombination rate. The recombination rate is the sum of rebinding rates from inside the protein (geminate) or from solution. Importantly, the decrease in photodissociation yield occurs on the same time scale as the increase in the photoproduct $\nu_{Fe\text{-}His}$ frequency. Thus the $\nu_{Fe\text{-}His}$ frequency

dx.doi.org/10.1021/ja210126j | J. Am. Chem. Soc. 2012, 134, 3461−3471

increases in concert with the CO rebinding rate, as the protein structure evolves.

d. UVRR Markers of Tertiary and Quaternary Structure. UVRR difference spectra were monitored after CO binding to deoxyHb gel (Figure 8) and eventually showed the same signals

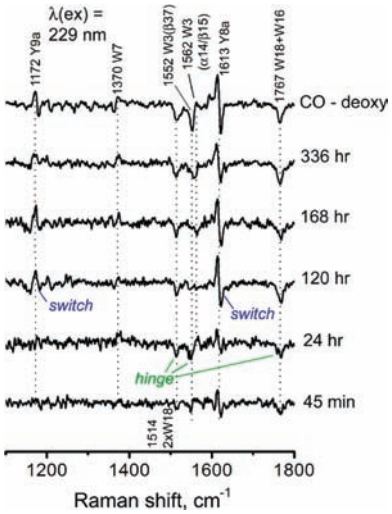

Figure 8. UVRR difference spectra (COHb minus deoxyHb) collected at the indicated times during the T to R conversion in sol–gels. A static CO-minus-deoxy difference spectrum of Hb in sol–gel is provided at the top for reference. Peaks assignable to interdimer (quaternary) H-bonds are labeled as in Figure 2.

as a static COHb minus the deoxyHb difference spectrum, indicating the breaking of hinge and switch T-state contacts. As in the R-T sequence (Figure 4), full development of the quaternary signals required an excess of 120 h. There is no discernible timing difference between the hinge and switch signals, indicating that the contacts break simultaneously, in contrast to their sequential formation in the R-T direction. Another contrast is that the spectra preceding the full development of quaternary signals do not contain signals associated with the tertiary Trp and Tyr interhelical H-bonds, as they do in the R-T sequence. Evidently these H-bonds are unperturbed during the T-R sequence. Instead, the spectra at 45 min and 24 h contain weak signals at the quaternary Trp and Tyr positions that eventually grow into the full R minus T signals. Thus the tertiary phase in the T-R sequence involves early weakening of the hinge and switch contacts, which later break in the quaternary phase.

It is during the tertiary phase, in which weak hinge and switch difference signals are observed, that the $\nu_{Fe\text{-}His}$ and photoproduct yield signals evolve toward the R-state values. This evolution is complete well before the full development of the quaternary signal.

DISCUSSION

$\nu_{Fe\text{-}His}$ Band Is a Marker of Heme Reactivity. Previous studies have correlated the deoxy-heme $\nu_{Fe\text{-}His}$ frequency with ligand affinity[69] or binding rate[70] in various Hb preparations. A lower frequency correlates with both the lower affinity and the lower binding rate. This correlation has a clear physical basis, since a lower frequency indicates protein-induced strain on the Fe–His bond, either directly via an altered conformation of the His side chain, or indirectly, via weakening of the His side chain H-bonding with an F helix residue.[71] The deoxy-heme Fe lies out of the heme plane toward the proximal side, and it must approach the plane more closely to bind exogenous ligand. Strain on the Fe–His bond therefore inhibits ligand binding. The low $\nu_{Fe\text{-}His}$ frequency (212 cm^{-1}) of deoxyHb is the most direct spectroscopic indication of molecular tension in the T state.

Our observation that the photolysis yield in CO-exposed deoxyHb gels declines with time and does so on the same time scale as the increase in photoproduct $\nu_{Fe\text{-}His}$ frequency supports this view. The photolysis yield declines because the geminate recombination rate increases as the low-affinity structure evolves toward the high-affinity structure, in response to the concomitant relaxation of the Fe–His bond. These data on a single, evolving native Hb preparation establish that $\nu_{Fe\text{-}His}$ directly reflects heme reactivity.

Heme Reactivity Is a Tertiary Property, within Either Quaternary Structure. The present data further establish that heme reactivity evolves faster than quaternary structure change. In earlier sol–gel studies Friedman and co-workers[57] found $\nu_{Fe\text{-}His}$ evolution on the same time scale that we observe, but they assumed that the later phase reflected quaternary structure change, following an earlier tertiary phase. Our UVRR analysis shows that in the R-T direction (deoxygenation of oxyHb), five days are required for markers of the T quaternary contacts to appear, whereas evolution of $\nu_{Fe\text{-}His}$ is completed within two days. Moreover, this evolution spans the entire range of values observed in static spectra of R- and T-state deoxyHb, 224–212 cm^{-1}. Since the quaternary structure remains R at the end of this evolution, we assign these frequencies to *r* and *t* tertiary structures. The implication is that the full heme tension seen in T-state Hb, as well as the accompanying reduction in heme reactivity, is in fact a *t* tertiary property.

The analysis of tertiary/quaternary separation is less clear-cut in the T-R direction (ligation of deoxyHb) because UVRR markers for loss of the T contacts begin to appear within 45 min. However, they are not fully developed for at least a week (Figure 8). Meanwhile the evolution of $\nu_{Fe\text{-}His}$ associated with the COHb photoproduct is again completed within two days (Figure 6), as is evolution of the photoproduct yield (Figure 7), both of which cover the full range of expected values between the T and R states. Thus tertiary evolution of heme reactivity precedes the full quaternary structure change, within the T as well as the R state.

These results directly support the tertiary two-state (TTS) model of cooperativity in Hb ligand binding, recently advanced by Eaton and co-workers.[31] This model posits that the Hb tetramer contains subunits in high- and low-affinity conformations, whose populations are biased by the quaternary structure. The change in quaternary structure is induced by the shifting population of *r* and *t* structures, as the subunits are successively ligated or deligated. Our results demonstrate that *r* and *t* tertiary structures can indeed be accommodated within both quaternary structures.

In principle, our RR spectra could be deconvoluted into *t* and *r* component spectra, in order to determine the time dependence of the *t* and *r* subunit populations. However, the $\nu_{Fe\text{-}His}$ band is too broad for this procedure, being in fact a composite of α and β chain bands, with different frequencies.[72,73] The time dependence of the $\nu_{Fe\text{-}His}$ band therefore represents the evolution of the *t* and *r* population average for both α and β chains.

How Does the Protein Control Heme Reactivity? In view of the correlation between changes in heme reactivity and

dx.doi.org/10.1021/ja210126j | J. Am. Chem. Soc. 2012, 134, 3461–3471

the $\nu_{Fe\text{-}His}$ frequency, we focus on how the Fe−His bond can be modulated by the protein during tertiary relaxation. It is clear that the mechanism must differ between the R and T states. The UVRR spectral changes during the course of $\nu_{Fe\text{-}His}$ evolution in gels are entirely different when monitored in R-T (deoxygenated oxyHb) or in T-R (CO-saturated deoxyHb) conversions. For R-state Hb we observe the same sequence of changes as in solution pump−probe studies of photodissociated COHb, namely, the appearance and disappearance of difference bands signaling the breaking of tertiary H-bonds between the A and E and between the F and H helices (Figure 4). For the T-state COHb, there are no transient signals at these positions, indicating that the tertiary H-bonds linking A−E and F−H helices remain intact throughout the time course of structural evolution. Rather, signals consistent with weakening of the T-state hinge and switch quaternary contacts appear rapidly after CO addition to encapsulated deoxyHb, as has been noted by Friedman and co-workers.[35] These signals (negative difference intensity at the W3 and Trp overtone and combination bands and a shift in the Y8a peak) eventually grow to intensities consistent with complete loss of these contacts, but only long after completion of the photoproduct $\nu_{Fe\text{-}His}$ evolution. The different course of events occurring upon tertiary structural change within the R and T states is shown schematically in Figure 9.

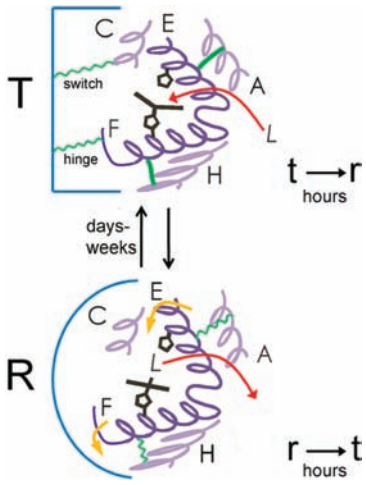

Figure 9. Model for uncoupling of tertiary and quaternary structural transitions in Hb sol−gels. T and R quaternary structures are indicated by square and semicircular outlines, respectively. The *t*−*r* tertiary transition, induced by addition of ligand ("L") to T-state deoxyHb (top) consists of weakening of the interdimer H-bonds (indicated by waved green lines) without altering the internal H-bonds (solid green lines) anchoring the E/F clamshell. The *r*−*t* tertiary transition, induced by removal of ligand from the R-state Hb (bottom), is manifest as breakage of the internal H-bonds, allowing rotation of the E and F helices as suggested by the curved gold arrows. See text for details.

To rationalize these results, we note that when crystal structures of ligated and unligated Hb are compared, a prominent feature is displacement of the F-helices, which contain the proximal histidines.[4] The F helices are constrained in the T state by intersubunit H-bonds at the $\alpha_1\beta_2$ interface (the hinge and switch contacts, Figure 1), which link the FG corner of each chain with the C helix of the other. Ligation in the T state is expected to strain these intersubunit contacts, as formation of the 6-coordinate, low-spin CO-heme draws the Fe into the heme plane and reorients the Fe−His bond, pulling on the F-helix. This sequence of events was anticipated many years ago in computational work by Gelin and colleagues,[74] who found that motions of the F-helices and FG-corners are required to compensate for heme motions and tilting induced by ligand binding. More recently, such F-helix motion has been directly observed by time-resolved crystallography following photolysis of CO from the α heme of a T-state hybrid Hb.[75] Furthermore, it is known that the hinge H-bond breaks under some conditions upon oxygenation of IHP-bound deoxyHb crystals.[76] Thus it is reasonable to observe weakening of the hinge and switch H-bonds upon CO binding to deoxyHb gels.

We infer that the strain on these intersubunit H-bonds reflects resistance to F-helix motion and is responsible for the low frequency of $\nu_{Fe\text{-}His}$ in the immediate photoproduct, which subsequently rises as the interfacial contacts weaken further, allowing greater F-helix motion. From the perspective of the TTS model, the subunits are all *t* in the initial T-state COHb, but the subunit population evolves toward *r*, as ligation forces work against the interfacial stress.

In the R-T direction (oxyHb deoxygenation), on the other hand, the hinge and switch H-bonds are absent, and the F-helix is initially unconstrained. Deligation, however, pushes on the F-helix as the Fe is driven out of the heme plane, and the Fe−His bond lengthens in the 5-coordinate, high-spin deoxy-heme. At the same time departure of the ligand from the heme pocket allows the distal E-helix to collapse toward the heme. Together, these motions produce a concerted rotation of the EF "clamshell". The breaking of the A−E and F−H interhelical H-bonds, detected in pump−probe UVRR difference spectra in solution, was viewed as reflecting the concerted EF rotation.[16] However, this interpretation now requires modification, in view of the evidence from the gel UVRR spectra that the A−E H-bond breaks well before the F−H H-bond. The A−E signal is already apparent 3 min after deoxygenation (Figure 4), within the initial phase of $\nu_{Fe\text{-}His}$ relaxation (τ_1 = 6 min, Figure 3). Development of the F−H signal starts at 45 min and takes about a day, during the second and third $\nu_{Fe\text{-}His}$ phases (2.8 and 15 h). We infer that EF helix rotation relaxes the Fe−His bond during the initial phase and is signaled by A−E H-bond loss alone. The subsequent F−H H-bond loss is associated with the later $\nu_{Fe\text{-}His}$ phases, when the Fe−His bond is becoming significantly strained. The F−H H-bond is at the FG corner (Figure 1), which is also the locus of the hinge (α chain) or switch (β chain) quaternary contacts. We suggest that the EF rotation impels subsequent F-helix displacement that strains the Fe−His bond and loosens the FG corner, allowing later formation of the T quaternary contacts.

In this interpretation, tertiary forces generated by ligation in the T state immediately weaken the quaternary contacts, allowing Fe−His bond contraction prior to the breaking of these contacts, whereas deligation in the R state impels displacements of the E and F helices that lengthen the Fe−His bond, prior to the formation of the T contacts.

IHP Affects Heme Reactivity within the R State. Encapsulating the effector molecule IHP along with oxyHb has a pronounced effect on heme reactivity. $\nu_{Fe\text{-}His}$ is lowered significantly, ~6 cm^{-1}, even in the oxyHb photoproduct (Figure 3), demonstrating that IHP binds to oxyHb in a manner that influences the heme. Friedman and co-workers have reported similar IHP-induced lowering for COHb photoproduct, both in solution and in gels.[77]

dx.doi.org/10.1021/ja210126j | *J. Am. Chem. Soc.* 2012, 134, 3461−3471

Following deoxygenation of the oxyHb gel, $\nu_{Fe\text{-}His}$ remains significantly lower in the presence of IHP and continues to decrease with time but levels off at the essentially same frequency, 212 cm^{-1}, as in the absence of IHP. This is also the equilibrium value for deoxyHb. We infer that IHP significantly lowers heme reactivity in the *r* but not the *t* structure, within the R quaternary state.

In contrast, co-encapsulation of IHP with T-state COHb has hardly any effect on the photopoduct $\nu_{Fe\text{-}His}$ either immediately or during the subsequent T-R evolution, except that the final value is slightly (2 cm^{-1}) lower than in the absence of IHP (Figure 6). Thus heme reactivity is unaffected by IHP in the *t* structure, and only slightly in the *r* structure within the T state.

This absence of significant effect in the T state is surprising in the light of the finding by Viappiani et al. that a combination of IHP and bezafibrate (another effector molecule) completely suppressed the faster R-like CO recombination rate in T-state COHb gels and effectively locked in the T-state recombination rate for weeks after CO addition.[31] Evidently the combination of the two effectors, which are known to act synergistically in solution, inhibited the formation of *r* subunits. The recombination study did not report the effect of IHP alone, suggesting that bezafibrate, which is known to bind at a different site than IHP, is critical to the observed inhibition. We were unable to study the effect of bezafibrate because its strong Raman signal interferes with the Hb spectra.

The classical role of IHP is to stabilize the T quaternary structure of Hb, by binding to cationic sites in its central cavity.[6] This cavity narrows in the R structure, expelling the IHP. Thus IHP has been thought to lower ligand affinity by selectively stabilizing the T state. The present data are uninformative about this effect, since the time scale for quaternary structure change is too long (and the time resolution of our UVRR method too coarse) in the sol−gel to detect any effect of IHP on the T−R transition rate.

However, accumulating evidence implicates an additional interaction of IHP in the R state. In particular, Yonetani has produced extensive evidence for effector-induced affinity changes within *both* quaternary states, and the effects are larger for the R state.[15] Also, Ho and co-workers[78] found that IHP greatly increases the NMR-detected microsecond−millisecond conformational exchange around the interdimer interface of COHb, with the greatest increases occurring in the F helix and FG-corner of the α chain,[78] regions that would be expected to influence $\nu_{Fe\text{-}His}$ relaxation (see above). In contrast, the effects of IHP on T-state dynamics were comparatively small,[78] consistent with our finding that IHP has little effect on the evolution of $\nu_{Fe\text{-}His}$ or photolysis yield in the T state (Figures 6 and 7).

Our results imply that IHP binds to R-state Hb in a manner that weakens the Fe−His bond, lowering heme reactivity. Surprisingly, the UVRR spectra are unaffected by IHP binding, in either the tertiary or quaternary phases. Thus the R-state interaction with IHP is quite specific to the heme and has no discernible influence on the helix motions. The structural basis for such an effect is uncertain. Perhaps IHP binding to R-state Hb introduces ionic forces that specifically alter the proximal histidine orientation or H-bonding. A similar effect is not operative in the T state. IHP may well stabilize the T structure, but it is without significant influence on the Fe−His bond.

CONCLUSIONS

Encapsulation in silica gel slows protein motion sufficiently to distinguish successive tertiary and quaternary phases in Hb. The combined application of visible and UV resonance Raman spectroscopy establishes the time scales for tertiary and quaternary motions along the allosteric pathway, in both the R-T and the T-R directions. On the R-T pathway, deligation induces displacement of the E and F helices, as in solution, breaking first A−E and then F−G interhelical H-bonds. In a subsequent step, these H-bonds reform, prior to the quaternary phase, in which the T interfacial contacts are established, first the hinge and then the switch. On the T-R pathway, heme ligation immediately weakens the T contacts, which then break in a much later step.

In both the R-T and T-R directions, the $\nu_{Fe\text{-}His}$ frequency, a monitor of heme reactivity, evolves over the full range of values characterizing the R and T states, long before the quaternary structure changes. This result implies that heme reactivity is controlled at the level of tertiary structure and supports the TTS ligand-binding model, in which high- and low-affinity subunits, having *r* and *t* tertiary structures, coexist within each quaternary structure.

In the R state, the allosteric effector molecule IHP lowers the $\nu_{Fe\text{-}His}$ frequency in the *r* but not the *t* tertiary structure. In the T state, IHP has little effect on either the *r* or the *t* $\nu_{Fe\text{-}His}$ frequency. While the classic role of IHP is to stabilize the T structure, it also binds to the R structure, where it lowers heme reactivity in *r* subunits. It does this without a discernible effect on the tertiary protein motions, presumably by specifically interacting with the heme in a manner that strains the Fe−His bond.

The present results provide a view of the mechanism of heme reactivity changes, as dictated by tertiary structure, along the allosteric trajectory of gel-encapsulated hemoglobin. The means by which these tertiary transitions bring about full quaternary change, however, remains unclear. In light of the recent finding of a two-step quaternary transition of Hb,[16,23,27,29] it will be of great interest to elucidate the mechanism of tertiary coupling to the quaternary transition, as well as to investigate any inequivalence of the α and β chains in these processes.

ASSOCIATED CONTENT

Supporting Information

Comparative low-frequency visible RR spectra of Hb in solution and gel, error surface analysis, and comparative UVRR spectra of Hb in solution and gel. This material is available free of charge via the Internet at http://pubs.acs.org.

AUTHOR INFORMATION

Corresponding Author

spiro@chem.washington.edu

ACKNOWLEDGMENTS

This work was supported by NIH Grant GM 25158. We thank Dr. Alexandra V. Soldatova and Dr. Mohammed Ibrahim for assistance with the purification of hemoglobin, and Dr. Thomas C. Squier for assistance with error surface analysis.

REFERENCES

(1) Monod, J.; Wyman, J.; Changeux, J. P. L *J. Mol. Biol.* **1965**, *12*, 88−118.

(2) Fermi, G.; Perutz, M. F.; Shaanan, B.; Fourme, R. *J. Mol. Biol.* **1984**, *175*, 159−174.
(3) Perutz, M. F.; Muirhead, H.; Cox, J. M.; Goaman, L. C. G. *Nature* **1968**, *219*, 131−139.
(4) Baldwin, J.; Chothia, C. *J. Mol. Biol.* **1979**, *129*, 175−200.
(5) Perutz, M. F.; Fermi, G.; Luisi, B.; Shaanan, B.; Liddington, R. C. *Acc. Chem. Res.* **1987**, *20*, 309−321.
(6) Perutz, M. F. L. *Annu. Rev. Physiol.* **1990**, *52*, 1−25.
(7) Safo, M. K.; Abraham, D. J. *Biochemistry* **2005**, *44*, 8347−8359 and references therein.
(8) Lukin, J. A.; Ho, C. *Chem. Rev.* **2004**, *104*, 1219−1230.
(9) Lukin, J. A.; Kontaxis, G.; Simplaceanu, V.; Yuan, Y.; Bax, A.; Ho, C. *Proc. Natl. Acad. Sci. U.S.A.* **2003**, *100*, 517−520.
(10) Shulman, R. G. *IUBMB Life* **2001**, *51*, 351−357.
(11) Song, X. J.; Yuan, Y.; Simplaceanu, V.; Sahu, S. C.; Ho, N. T.; Ho, C. *Biochemistry* **2007**, *46*, 6795−6803.
(12) Eaton, W. A.; Henry, E. R.; Hofrichter, J.; Bettati, S.; Viappiani, C.; Mozzarelli, A. *IUBMB Life* **2007**, *59*, 586−599.
(13) Henry, E. R.; Bettati, S.; Hofrichter, J.; Eaton, W. A. *Biophys. Chem.* **2002**, *98*, 149−164.
(14) Lee, A. W. M.; Karplus, M. *Proc. Natl. Acad. Sci. U.S.A.* **1983**, *80*, 7055−7059.
(15) Yonetani, T.; Park, S.; Tsuneshige, A.; Imai, K.; Kanaori, K. *J. Biol. Chem.* **2002**, *277*, 34508−34520.
(16) Balakrishnan, G.; Case, M. A.; Pevsner, A.; Zhao, X.; Tengroth, C.; McLendon, G. L.; Spiro, T. G. *J. Mol. Biol.* **2004**, *340*, 843−856.
(17) Friedman, J. M.; Rousseau, D. L.; Ondrias, M. R. *Annu. Rev. Phys. Chem.* **1982**, *33*, 471−491.
(18) Goldbeck, R. A.; Paquette, S. J.; Bjorling, S. C.; Kliger, D. S. L. *Biochemistry* **1996**, *35*, 8628−8639.
(19) Hofrichter, J.; Sommer, J. H.; Henry, E. R.; Eaton, W. A. *Proc. Natl. Acad. Sci. U.S.A.* **1983**, *80*, 2235−2239.
(20) Jayaraman, V.; Rodgers, K. R.; Mukerji, I.; Spiro, T. G. *Science* **1995**, *269*, 1843−1848.
(21) Sawicki, C. A.; Gibson, Q. H. *J. Biol. Chem.* **1976**, *251*, 1533−1542.
(22) Chakrapani, S.; Auerbach, A. *Proc. Natl. Acad. Sci. U.S.A.* **2005**, *102*, 87−92.
(23) Goldbeck, R. A.; Esquerra, R. M.; Kliger, D. S. *J. Am. Chem. Soc.* **2002**, *124*, 7646−7647.
(24) Jones, C. M.; Ansari, A.; Henry, E. R.; Christoph, G. W.; Hofrichter, J.; Eaton, W. A. *Biochemistry* **1992**, *31*, 6692−6702.
(25) Rodgers, K. R.; Su, C.; Subramaniam, S.; Spiro, T. G. *J. Am. Chem. Soc.* **1992**, *114*, 3697−3709.
(26) Schiro, G.; Cammarata, M.; Levantino, M.; Cupane, A. *Biophys. Chem.* **2005**, *114*, 27−33.
(27) Cammarata, M.; Levantino, M.; Wulff, M.; Cupane, A. *J. Mol. Biol.* **2010**, *400*, 951−962.
(28) Spiro, T. G.; Balakrishnan, G. *J. Mol. Biol.* **2010**, *400*, 949−950.
(29) Fischer, S.; Olsen, K. W.; Nam, K.; Karplus, M. *Proc. Natl. Acad. Sci. U.S.A.* **2011**, *108*, 5608−5613.
(30) Fischer, S.; Karplus, M. *Chem. Phys. Lett.* **1992**, *194*, 252−261.
(31) Viappiani, C.; Bettati, S.; Bruno, S.; Ronda, L.; Abbruzzetti, S.; Mozzarelli, A.; Eaton, W. A. L. *Proc. Natl. Acad. Sci. U.S.A.* **2004**, *101*, 14414−14419.
(32) Shibayama, N.; Saigo, S. *J. Am. Chem. Soc.* **1999**, *121*, 444−445.
(33) Samuni, U.; Roche, C. J.; Dantsker, D.; Juszczak, L. J.; Friedman, J. M. *Biochemistry* **2006**, *45*, 2820−2835.
(34) Samuni, U.; Juszczak, L.; Dantsker, D.; Khan, I.; Friedman, A. J.; Perez-Gonzalez-De-Apodaca, J.; Bruno, S.; Hui, H. L.; Colby, J. E.; Karasik, E.; Kwiatkowski, L. D.; Mozzarelli, A.; Noble, R.; Friedman, J. M. *Biochemistry* **2003**, *42*, 8272−8288.
(35) Samuni, U.; Dantsker, D.; Juszczak, L. J.; Bettati, S.; Ronda, L.; Mozzarelli, A.; Friedman, J. M. *Biochemistry* **2004**, *43*, 13674−13682.
(36) Khan, I.; Shannon, C. F.; Dantsker, D.; Friedman, A. J.; Perez-Gonzalez-de-Apodaca, J.; Friedman, J. M. *Biochemistry* **2000**, *39*, 16099−16109.
(37) Juszczak, L. J.; Friedman, J. M. *J. Biol. Chem.* **1999**, *274*, 30357−30360.
(38) Riggs, A. *Methods Enzymol.* **1981**, *76*, 5−29.
(39) Antonini, E.; Brunori, M. *Hemoglobin and myoglobin in their reactions with ligands [by] Eraldo Antonini and Maurizio Brunori*; North-Holland Pub. Co.: Amsterdam, 1971.
(40) Friedman, J. M.; Lyons, K. B. *Nature* **1980**, *284*, 570−572.
(41) Zhao, X. J.; Chen, R. P.; Tengroth, C.; Spiro, T. G. *Appl. Spectrosc.* **1999**, *53*, 1200−1205.
(42) *CRC handbook of chemistry and physics: a ready-reference book of chemical and physical data*, 86th ed.; Lide, D. R., Ed.; CRC Press: Boca Raton, 2005.
(43) Beechem, J. M.; Haas, E. *Biophys. J.* **1989**, *55*, 1225−1236.
(44) Spiro, T. G.; Strekas, T. C. *J. Am. Chem. Soc.* **1974**, *96*, 338−345.
(45) Spiro, T. G.; Li, X. Y. In *Biological Application of Raman Spectroscopy*; Spiro, T. G., Ed.; John Wiley & Sons: 1987; Vol. 3, pp 1−37.
(46) Kitagawa, T.; Nagai, K.; Tsubaki, M. *FEBS Lett.* **1979**, *104*, 376−378.
(47) Walters, M. A.; Spiro, T. G. *Biochemistry* **1982**, *21*, 6989−6995.
(48) Ondrias, M. R.; Rousseau, D. L.; Shelnutt, J. A.; Simon, S. R. *Biochemistry* **1982**, *21*, 3428−3437.
(49) Friedman, J. M.; Scott, T. W.; Stepnoski, R. A.; Ikedasaito, M.; Yonetani, T. *J. Biol. Chem.* **1983**, *258*, 564−572.
(50) Kitagawa, T. *Prog. Biophys. Mol. Biol.* **1992**, *58*, 1−18.
(51) Austin, J. C.; Rodgers, K. R.; Spiro, T. G. In *Biomolecular Spectroscopy Part A*; Clark, R. J. H., Hester, R. E., Eds.; John Wiley & Sons Ltd: 1993; pp 55−127.
(52) Asher, S. A. *Annu. Rev. Phys. Chem.* **1988**, *39*, 537−588.
(53) Balakrishnan, G.; Tsai, C. H.; Wu, Q.; Case, M. A.; Pevsner, A.; McLendon, G. L.; Ho, C.; Spiro, T. G. *J. Mol. Biol.* **2004**, *340*, 857−868.
(54) Hu, X. H.; Spiro, T. G. *Biochemistry* **1997**, *36*, 15701−15712.
(55) Kneipp, J.; Balakrishnan, G.; Spiro, T. G. *J. Phys. Chem. B* **2004**, *108*, 15919−15927.
(56) Nagatomo, S.; Nagai, M.; Kitagawa, T. *J. Am. Chem. Soc.* **2011**, *133*, 10101−10110.
(57) Das, T. K.; Khan, I.; Rousseau, D. L.; Friedman, J. M. L. *Biospectroscopy* **1999**, *5*, S64−S70.
(58) Wang, D. J.; Zhao, X. J.; Shen, T. J.; Ho, C.; Spiro, T. G. *J. Am. Chem. Soc.* **1999**, *121*, 11197−11203.
(59) Kneipp, J.; Balakrishnan, G.; Chen, R. P.; Shen, T. J.; Sahu, S. C.; Ho, N. T.; Giovannelli, J. L.; Simplaceanu, V.; Ho, C.; Spiro, T. G. *J. Mol. Biol.* **2006**, *356*, 335−353.
(60) Rodgers, K. R.; Spiro, T. G. *Science* **1994**, *265*, 1697−1699.
(61) Guallar, V.; Jarzecki, A. A.; Friesner, R. A.; Spiro, T. G. *J. Am. Chem. Soc.* **2006**, *128*, 5427−5435.
(62) Kachalova, G. S.; Popov, A. N.; Bartunik, H. D. *Science* **1999**, *284*, 473−476.
(63) Sato, A.; Gao, Y.; Kitagawa, T.; Mizutani, Y. *Proc. Natl. Acad. Sci. U.S.A.* **2007**, *104*, 9627−9632.
(64) Zhao, X. J.; Chen, R. P.; Raj, V.; Spiro, T. G. *Biopolymers* **2001**, *62*, 158−162.
(65) Spiro, T. G.; Wasbotten, I. H. *J. Inorg. Biochem.* **2005**, *99*, 34−44.
(66) Ronda, L.; Abbruzzetti, S.; Bruno, S.; Bettati, S.; Mozzarelli, A.; Viappiani, C. *J. Phys. Chem. B* **2008**, *112*, 12790−12794.
(67) Xu, C. L.; Ibrahim, M.; Spiro, T. G. *Biochemistry* **2008**, *47*, 2379−2387.
(68) Balakrishnan, G.; Zhao, X.; Podstawska, E.; Proniewicz, L. M.; Kincaid, J. R.; Spiro, T. G. *Biochemistry* **2009**, *48*, 3120−3126.
(69) Matsukawa, S.; Mawatari, K.; Yoneyama, Y.; Kitagawa, T. *J. Am. Chem. Soc.* **1985**, *107*, 1108−1113.
(70) Friedman, J. M.; Scott, T. W.; Fisanick, G. J.; Simon, S. R.; Findsen, E. W.; Ondrias, M. R.; Macdonald, V. W. *Science* **1985**, *229*, 187−190.
(71) Scherlis, D. A.; Marti, M. A.; Ordejon, P.; Estrin, D. A. *In. J. Quant. Chem.* **2002**, *90*, 1505−1514.
(72) Nagai, K.; Kitagawa, T. *Proc. Natl. Acad. Sci. U.S.A.* **1980**, *77*, 2033−2037.

(73) Balakrishnan, G.; Ibrahim, M.; Mak, P. J.; Hata, J.; Kincaid, J. R.; Spiro, T. G. *J. Biol. Inorg. Chem.* **2009**, *14*, 741−750.
(74) Gelin, B. R.; Lee, A. W. M.; Karplus, M. *J. Mol. Biol.* **1983**, *171*, 489−559.
(75) Adachi, S.; Park, S. Y.; Tame, J. R. H.; Shiro, Y.; Shibayama, N. *Proc. Natl. Acad. Sci. U.S.A.* **2003**, *100*, 7039−7044.
(76) Kavanaugh, J. S.; Rogers, P. H.; Arnone, A. *Biochemistry* **2005**, *44*, 6101−6121.
(77) Peterson, E. S.; Shinder, R.; Khan, I.; Juczszak, L.; Wang, J. Q.; Manjula, B.; Acharya, S. A.; Bonaventura, C.; Friedman, J. M. *Biochemistry* **2004**, *43*, 4832−4843.
(78) Song, X. J.; Simplaceanu, V.; Ho, N. T.; Ho, C. *Biochemistry* **2008**, *47*, 4907−4915.